Available online at www.sciencedirect.com
ScienceDirect
Trans. Nonferrous Met. Soc. China 33(2023) 2698−2711
Transactions of Nonferrous Metals Society of China
www.tnmsc.cn

Effect of discrete Cr nano-nuclei on stripping property and resistivity of ultrathin Cu foil

Guang YANG[1], Yue HUI[1], Ju CHEN[1], Bo LI[1], Jian-hua CHEN[2], Kai LIU[2], Gui-de LIANG[2], Ding-rong DENG[1]

1. College of Marine Equipment and Mechanical Engineering, Jimei University, Xiamen 361021, China;
2. Fujian Yegood Technology Co., Ltd., Jinjiang 362241, China

Received 23 March 2022; accepted 26 July 2022

Abstract: An electrochemical deposition strategy for discrete Cr nano-nuclei to achieve ultrathin Cu foil stripping was proposed. The results indicated that this method could be utilized to prepare Cu foils with a thickness of about 1.34 μm. The Cr discrete nucleus density directly affects the stripping performance, surface roughness, and resistivity of Cu foils. Under our experimental conditions, the stripping performance of Cu foil was the best at a Cr discrete nucleus density of 15.7×10^9 cm^{-2} and resistivity of 4.95×10^{-7} Ω·m, 9.2% lower than that of conventional Cr coating of 0.67 μm in thickness and 15.8% lower than that of the coating with potassium dichromate, and the tensile strength exceeds 248.80 MPa.

Key words: electrodeposition; Cu foils; discrete nano-nuclei; stripping; resistivity

1 Introduction

Cu foils are frequently used in electronics due to their superior electrical conductivity, thermal conductivity, and high-temperature resistance. Due to the global demand for miniaturization, lightweight and multi-functional electronic components, the demand for thickness Cu foil with a thickness less than 6 μm (a Cu foil with a thickness less than 12 μm is defined as ultrathin) increases significantly [1−8]. Cu foils are typically made through electrodeposition or rolling annealing. Although producing small thickness Cu foil with rolling annealing equipment is difficult, electrodeposition is an efficient method for producing thin Cu foil. Electrodeposition produces ultrathin Cu foil by reducing Cu ions in the electrolyte and depositing it on the substrate.

Stripping layers technology is widely used to peel Cu foils successfully. Stripping layers are classified as organic, inorganic, or composite based on their production mechanism and composition [5]. WEI et al [8] successfully prepared Cu foil with a small thickness of 1.1 μm using chitosan with a hydroxyl group as the organic stripping layer. Nonetheless, the conductivity of Cu foil is poor due to organic matter adhering to Cu foils. To achieve the stripping of Cu foils, LEE et al [9] applied a layer of potassium dichromate solution to the mold. However, the hexavalent chromium in potassium dichromate is a carcinogenic chemical. Its coating could not control the bonding force between the substrate and Cu foils, resulting in an unstable stripping effect [10]. To prevent Zn diffusion due to too long storage time, TAN et al [11] proposed a Zn−Ni−P−La in the production of Cu foil alloy by incorporating rare earth lanthanum in the coating to fine coating crystallization. However, this method belongs to various alloy electroplating, and its formula and process are relatively complex.

As a result, preparing small thickness Cu foils

Corresponding author: Guang YANG, Tel: +86-18750942172, E-mail: yangg@jmu.edu.cn
DOI: 10.1016/S1003-6326(23)66291-0

with cost-effective and efficient methods to meet performance requirements while also achieving green environmental protection remains a challenge. In precision electroforming optical molds, YANG et al [12] developed the assisted demolding technology of electrodeposition discrete Pb nuclei. The fabrication process is straightforward. As a heavy metal, lead is unsuitable for popularization and industrial use. However, the method of employing discrete metal nuclei oxide to passivate the surface of the substrate is worth understanding. Currently, none of the research groups have investigated discrete nuclei as a means of stripping Cu foil layers. The discrete nuclei used as stripping layers must meet conditions like being simple in depositing discrete metal nuclei on the substrate, controllable nucleus density, facilitating the oxidation of reduced metal nuclei, and the metal used to form discrete nuclei must not be heavy metal, non-toxic, and environment friendly. Cr_2O_3 has a good passivation effect on a Cu substrate, which is widely used to prevent metal corrosion [13]. Cr discrete core is deposited on the substrate, and Cr combines with the O element on the substrate's surface to form Cr_2O_3. Cr_2O_3 reduces the substrate's surface energy, reducing the binding force between the substrate and the Cu foil, which is why the Cr discrete core is conducive to the stripping of Cu foil. This is the research outcome of our recent article [14], and it shows why Cr_2O_3 lowers the bonding force between the substrate and the Cu foil at the atomic level.

Electrodeposition is an effective metal reduction technology that can deposit mono-crystalline nuclei with even distribution on the substrate. One advantage of electrodeposition is that nucleus density and size can be effectively controlled by adjusting the deposition parameters [12]. The metal Cr obtained by electrodeposition has a small grain size, uniform distribution, and a high deposition rate, making it ideal for preparing functional layers in the form of discrete nuclei.

In this study, Cu foils are stripped by electrodeposition of discrete Cr nano-nuclei. We found that the different densities of the Cr nuclei influenced the stripping force and resistivity of Cu foils, which had never been explored before. Replacing hexavalent chromium with uniformly distributed Cr nuclei electrodeposited by trivalent chromium is environmentally friendly and aids in reducing the diffusion of Cr element to Cu foils and resistivity of Cu foils. In addition to the stripping properties and resistivity, the effect of Cr nucleus density on tensile strength and surface roughness of Cu foils is also investigated. These analyses serve as a reference for the utility of preparing Cu foils.

2 Experimental

The first step of the experiment is to make Cr discrete nuclei on the surface of Cu foil. First, a polished copper sheet was immersed in a 10% phosphoric acid solution for 5 min to remove the oxide layer before being washed numerous times with deposited water. Then, using a copper sheet as the cathode and a titanium basket as the anode, uniform discrete Cr nuclei on the surface of the copper sheet were reduced after 3 s of electrodeposition. The second step is to deposit Cu foil on the surface of the copper sheet with Cr nuclei. First, a copper sheet with Cr nuclei was used as the cathode, and the titanium basket with 3 wt.% phosphorous copper was used as the anode. After 60 s of electrodeposition, a Cu foil thickness of about 1.34 mm was obtained. Figure 1 shows the schematic diagram of discrete Cr nano-nuclei and Cu foil preparation.

2.1 Preparation of discrete Cr nano-nuclei

Discrete Cr nano-nuclei were produced by electrodeposition. The anode was a titanium basket, the base was a Cu sheet, and the surface of the copper sheet was polished with a P-1-type metallographic sample polishing machine. Cr nuclei were deposited by constant potential deposition using deposition potentials of −1.1, −1.2, −1.3, −1.4, and −1.5 V, respectively. The chemical reaction equations used are as follows:

$$Cr^{3+} + 6H_2O = [Cr(H_2O)_6]^{3+} \quad (1)$$

$$[Cr(H_2O)_6]^{3+} + NH_2CH_2COO^- = [Cr(H_2O)_5NH_2CH_2COO]^{2+} + H_2O \quad (2)$$

$$2[Cr(H_2O)_5NH_2CH_2COO]^{2+} + 2Cl^- = 2[Cr(H_2O)_5NH_2CH_2COO]^{+} + Cl_2 \quad (3)$$

$$[Cr(H_2O)_5NH_2CH_2COO]^{+} + 2Cl^- = Cr + NH_2CH_2COO^- + Cl_2 + 5H_2O \quad (4)$$

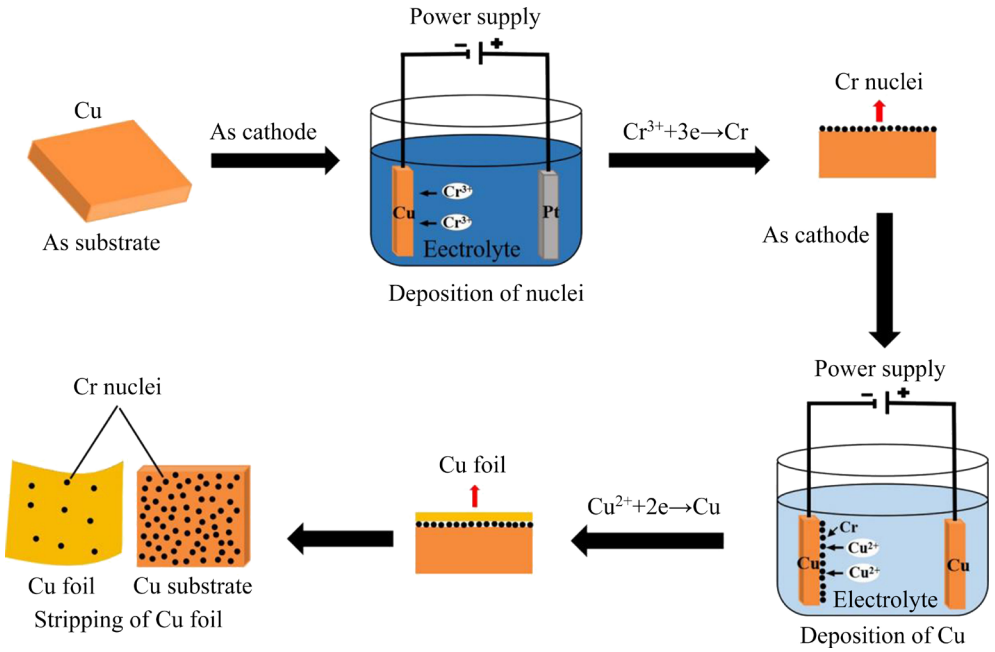

Fig. 1 Schematic diagram of discrete Cr nano-nuclei and Cu foils preparation

The composition of the electroplating solution and electrodeposition conditions are shown in Table 1.

Table 1 Parameters of electrodeposition process for Cr nano-nuclei

Parameter	Value
$Cr_2(SO_4)_3$ concentration/(g·L^{-1})	19−30
NH_4Cl concentration/(mL·L^{-1})	200−300
H_3BO_3 concentration/(mg·L^{-1})	60−100
$C_2H_5NO_2$ concentration/(mL·L^{-1})	20−50
Temperature/°C	43
pH	3.0−3.5
Time/s	3

2.2 Preparation of Cu foils

The prepared samples were fixed to the cathode of the electroforming tank for the electrodeposition of Cu foils. $CuSO_4$ electroplating solution was used as the electroforming solution, and a 3 wt.% phosphor copper sheet was used as an anode material. The cathode to anode area ratio was about 1:1.5, the spacing was 5.0 cm, and the drug dosage and electroforming parameter setting are shown in Table 2. Cu foil is made after deposition, passivation, washing, drying, and stripping. The chemical reaction equation used is as follows:

$$Cu^{2+}+2Cl^{-}=Cu+Cl_2 \quad (5)$$

Table 2 Electrodeposition process parameters for Cu foil

Parameter	Value
$CuSO_4·5H_2O$ concentration/(g·L^{-1})	195−225
H_2SO_4 concentration/(mL·L^{-1})	28−37
Cl^- concentration/(mg·L^{-1})	50−100
Hardener concentration/(mg·L^{-1})	2
Current density/(A·dm^{-2})	5−10
Time/s	60
Temperature/°C	25
pH	3.5−4.0

2.3 Characterization

X-ray diffraction (XRD) tests were performed on the near and far sides of the Cu foils. The crystal structure of Cu foil was determined using XRD (X' PertPro, 40 kV working voltage, 30 mA current, Netherlands), equipped with a Cu K_α line as a radiation source (λ=0.154 mm). The range of 2θ angle was 5°−85° and the diffraction angle scanning speed was 0.05 (°)/s. The thickness of Cu foils was measured by ion beam scanning electron microscope (Sigma−550, Carl Zeiss, Crossbeam, Germany). The tensile strength of the three samples was measured using a PT−305 electronic tensile testing machine (tensile speed: 10 mm/min), and the average value was taken. The samples measure 1.2 cm in length, 1.4 cm in width, and 1.34 mm in thickness. Before the test, two strips of adhesive

tape, 4 cm in length and 2 cm in width, were applied to both ends of the Cu foil to secure it to the testing device. The thickness and the resistivity of the Cu foils were measured using a multimeter in triplicate values. The surface roughness was measured using a confocal microscope (VK-X1000, Japan). The surface roughness of each sample was assessed at five different positions, and the average value was calculated. The surface information of the modified sample was obtained by analyzing the substrate surface with XPS technology. XPS spectra were generated using PHI Quantum 2000 (Physical electronics Co., Ltd., USA) system with an Al K_α line source ($h\nu$=1486.6 eV) at a 45° incident angle. The analysis chamber had a base vacuum of about 2.0×10^{-7} Pa. Two spectra were recorded: a wide-range survey with a pass energy of 187.85 eV and a resolution of 1 eV and a narrow range survey with a pass energy of 29.35 eV and a resolution of 0.125 eV. The narrow spectra of C 1s and O 1s were measured once every minute of sputtering, and all spectra were referenced to the C 1s line of 284.7 eV. Peak fitting was performed using the VG Eclipse 3.1 software after Shirley baseline background subtraction. The peak areas of the high-resolution spectra and the Scofield sensitivity factors were used to perform quantitative surface and interface analyses [15,16]. The grain distribution of Cu foil was analyzed using a single-sphere differential microscope (FEI Titan G2 60-300). An ion thinning device (Gatan PIPS 695) was used to thin the Cu foil.

3 Results

3.1 Morphology and elemental distribution of samples

The surface morphology of the Cu sheet was photographed after deposition using field emission scanning electron microscopy, and the number of Cr nuclei was calculated using Image Pro Plus software. Cr nucleus density was determined to be 2.61×10^9, 4.47×10^9, 5.00×10^9, 9.98×10^9 and 15.7×10^9 cm^{-2} (Samples 1−5), respectively, corresponding to potentials of −1.1, −1.2, −1.3, −1.4, and −1.5 V, while Cr nuclei size ranged from 12 to 30 nm. Stripped Cu foils exhibit different curly states when deposited on substrates with varying Cr nucleus densities, as shown in Figs. 2(f)−(j). Figures 2(k)−(o) show the SEM images of Cu foils corresponding to different Cr nucleus densities in Figs. 2(a)−(e). Figures 2(p)−(t) show the morphology of Cu substrate corresponding

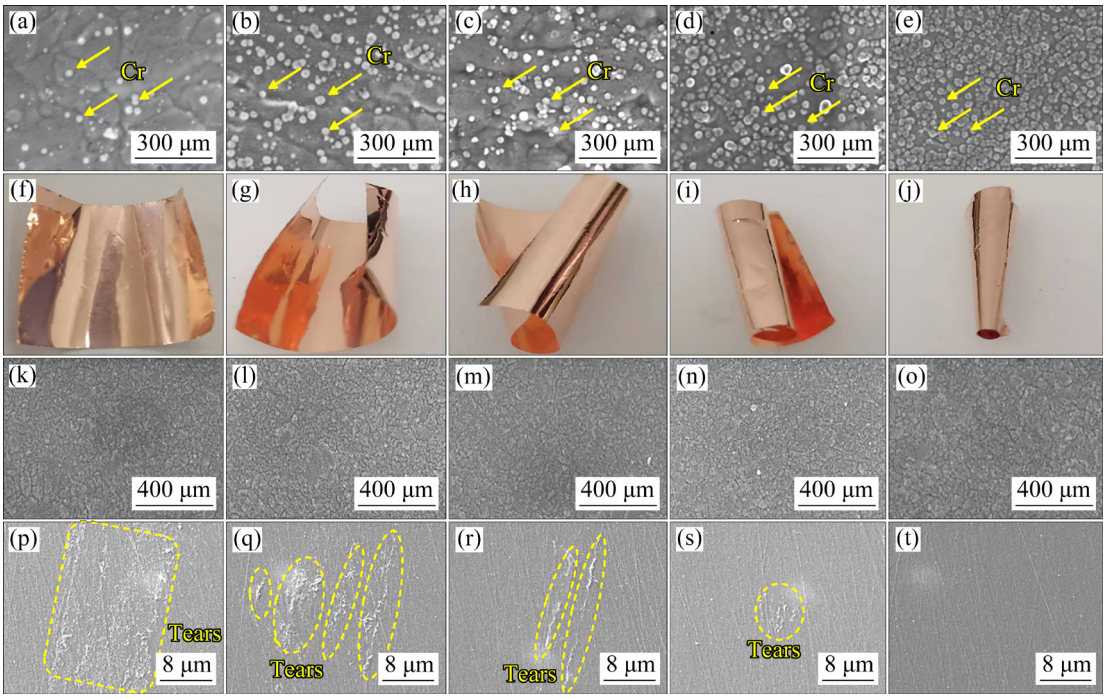

Fig. 2 SEM images of substrate deposited Cr nuclei: (a−e) At deposition potentials of −1.1, −1.2, −1.3, −1.4 and −1.5 V, respectively; (f−j) Morphology of stripped Cu foils corresponding to different Cr nucleus densities in (a−e); (k−o) SEM images of Cu foils corresponding to different Cr nucleus densities in (a−e); (p−t) Morphology of substrate separated from Cu foil corresponding to different Cr nucleus densities in (a−e)

to different Cr nucleus densities in Figs. 2(a)−(e). As shown in Figs. 2(f)−(j), the higher the density of Cr nucleus, the more crimped the Cu foil. According to the surface morphology of the separated substrate, the higher the density of the Cr nucleus is, the fewer the microscopic tears are, and the smoother the surface of the substrate is.

In Fig. 3(a), the elemental composition of the sample surface shows that, in addition to the C and O elements, the Cr element peak is very visible. The appearance of carbon elements is caused by contamination of the air-exposed substrate.

3.2 XRD results

The XRD patterns of Cu foils near the substrate side are shown in Fig. 4 and far from substrate sides are shown in Fig. 5. As shown in Fig. 4, the maximum texture of Cu substrate was found to be (200) and (111) for Cu foils near the substrate. With the increase of Cr nucleus density, the diffraction peak of the (111) crystal plane shifts to the right, as shown in Fig. 4(b), indicating that the lattice constant of Cu foils decreases as Cr nucleus density increases [17−20]. Furthermore, with the increase of Cr nucleus density, the diffraction peak

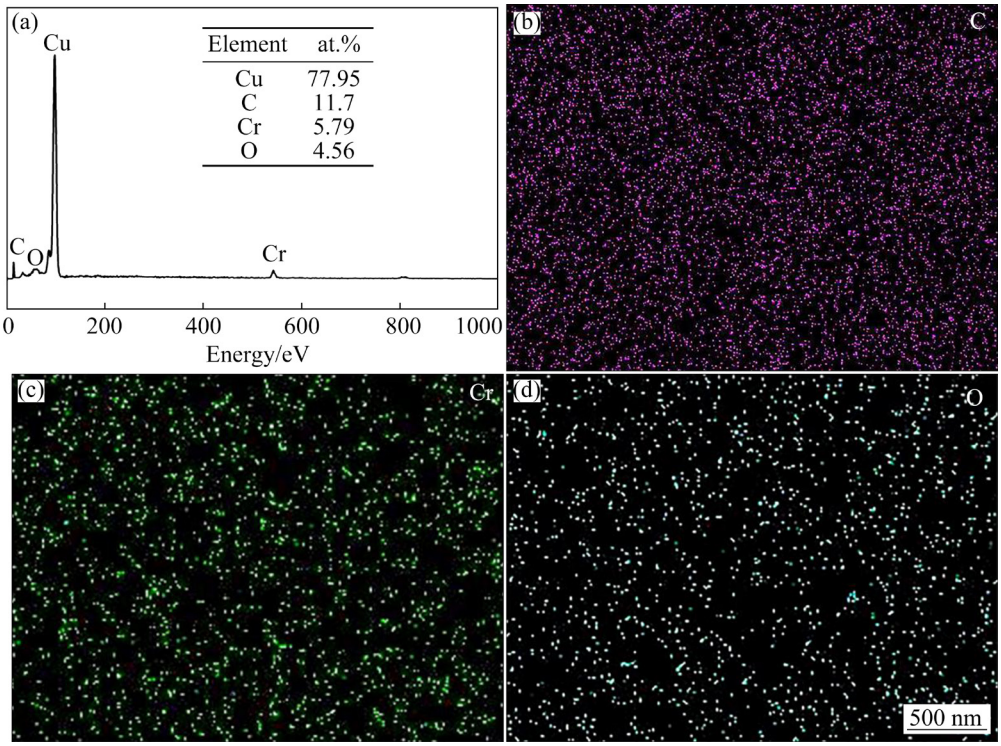

Fig. 3 EDX spectrum on Cu substrate with Cr discrete nuclei: (a) Peak intensity and molar fraction of surface composition; (b, c, d) Distribution of C, Cr and O elements, respectively

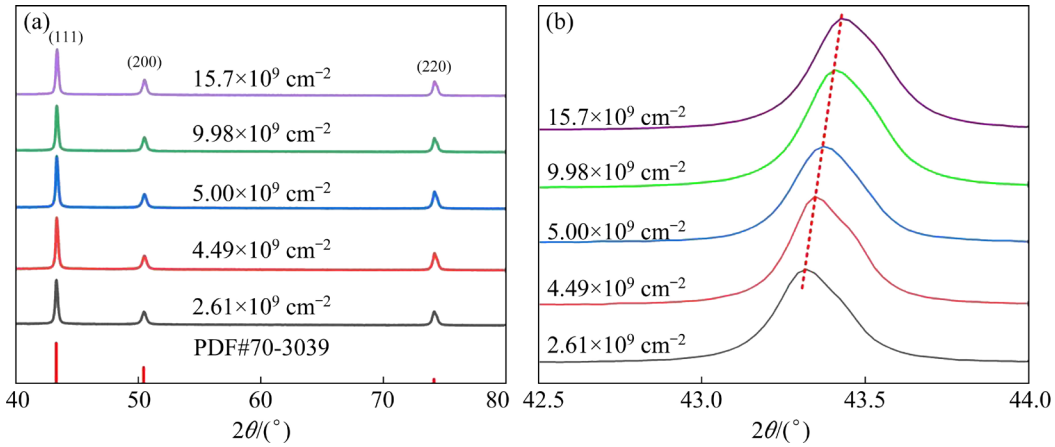

Fig. 4 XRD patterns of Cu foils with Cr discrete nuclei near substrate side: (a) Full XRD patterns of Cu foil; (b) Patterns of (111) crystal plane

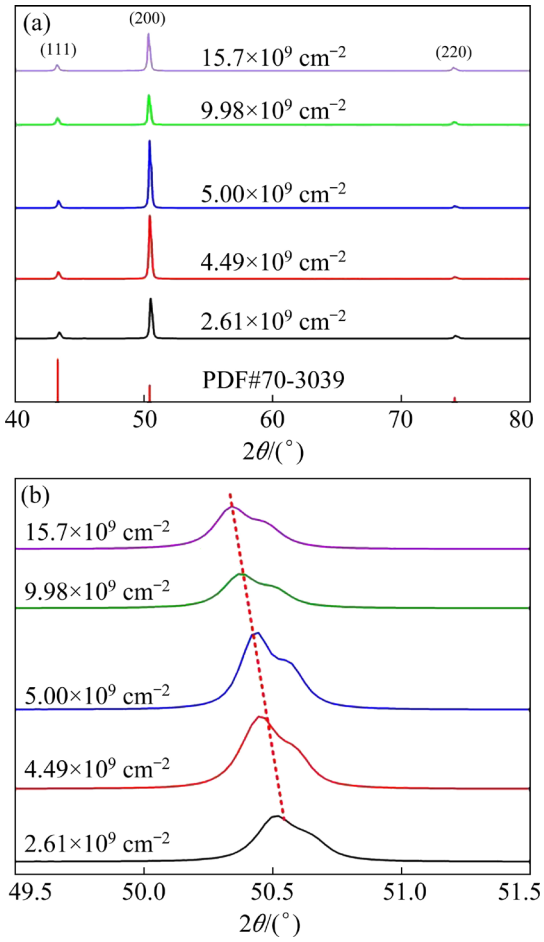

Fig. 5 XRD patterns of Cu foils with Cr discrete nuclei far from substrate sides: (a) Full XRD patterns of Cu foil; (b) Patterns of (200) crystal plane

of the (200) crystal plane shifts to the left, as shown in Fig. 5(b), indicating that the lattice constant of Cu foils increases as Cr nucleus density increases. When electrodeposition commences, the crystal orientation of Cu foils is the (111) plane. As the electrodeposition proceeded, electrodeposited fresh atoms were incapable of migrating to the (111) plane, and some of them would rest on the (200) plane, which consequently accelerated the growth of the (200) plane and influenced the preferred orientation. As a result, Cu foils on the far sides of the substrate exhibit obvious (200) preferred orientation. The crystal orientation of the electrodeposited Cu foils on the far substrate sides is supposed to be controlled by the electrodeposition parameters, and these results are in agreement with the results in Refs. [21,22]. The change of the lattice constant of copper foils affects the grain size, which affects the tensile strength of copper foils.

3.3 XPS results

XPS measurements in Fig. 6 revealed that the Cu substrate deposited with Cr nuclei had a distinct peak of Cr element when compared to the pure Cu substrate. Only the C 1s and O 1s peaks were visible on the untreated Cu substrate surface at 284.8 and 532.0 eV, respectively. With increasing Cr nucleus density, the intensity of coating surface peak O 1s increases, while the strength of the C 1s peak decreases.

3.4 Electric conductivity of Cu foils

The resistance of Cu foils was measured using a multimeter and the resistivity of Cu foils was calculated. The average value was calculated after getting three values. The resistivity of Cu foils corresponding to different Cr nucleus densities is shown in Fig. 7, which is similar to a linear relationship.

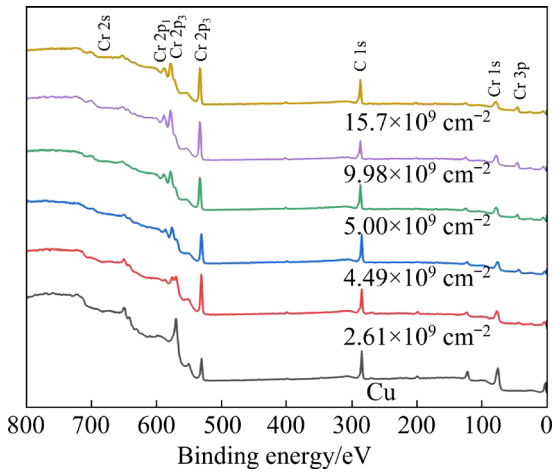

Fig. 6 Wide range XPS spectra of Cu substrate surface

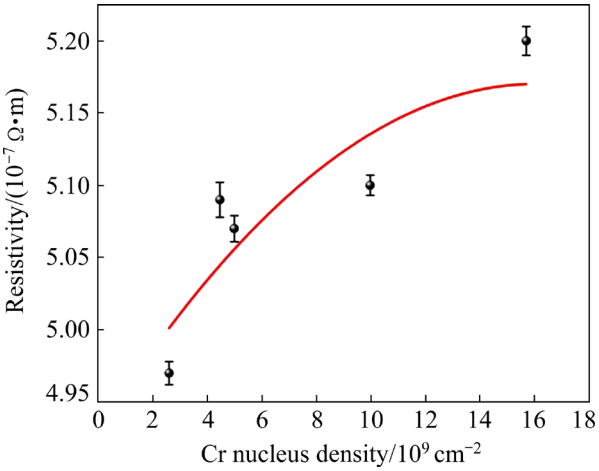

Fig. 7 Fitting curves of Cr nucleus density and resistivity with Cr discrete nuclei

3.5 Tensile strength of Cu foils

The grain size of Cu foils was determined using the XRD test. The relationship between Cr nucleus density and Cu foil grain size is clarified in this section. Figure 8(a) illustrates the relationship between nucleus density and grain size of near substrate Cu foils, and Fig. 8(b) shows the relationship between Cr nucleus density and the average gain size of far from substrate Cu foils.

It is clear that Cr dispersion significantly impacts the crystallization of Cu foils near the substrate side. The grain size of Cu foils near the substrate side decreases as the density of Cr nuclei increases. Figure 8(b) illustrates that the grain size of far substrate Cu foils is not regular. The reason for this is that the electroplating environment greatly influences the grain size of Cu foils far from substrate side.

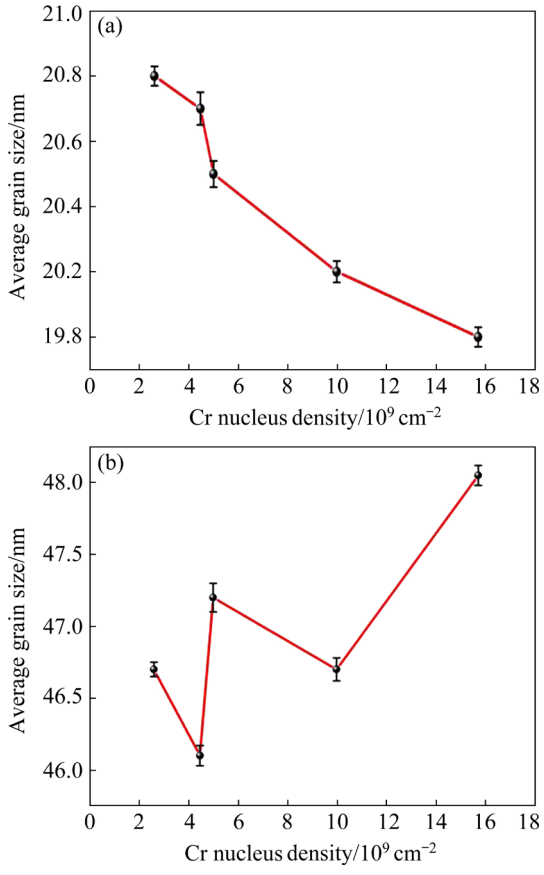

Fig. 8 Relationship between Cr nucleus density and grain size of Cu foils: (a) Side near Cu foil; (b) Side far from Cu foil

The tensile strength of Cu foil is an important factor in determining its quality. The tensile strength of the three samples was measured using a testing machine (tensile speed preset at 10 mm/min), and the average value was taken. The load−displacement curves of Cu foil are shown in Fig. 9. The tensile strength of Cu foils with a thickness of 1.34 μm is 78.60−248.80 MPa. According to the Hall−Petch strength theory, decreasing the average grain size increases the strength of Cu foils [23−25]. The tensile strength of Cu foil prepared by deposition of Cr nucleus density of 15.7×10^9 cm^{-2} on the substrate increases by 215% compared with that prepared by deposition of Cr nucleus density of 2.61×10^9 cm^{-2} on the substrate.

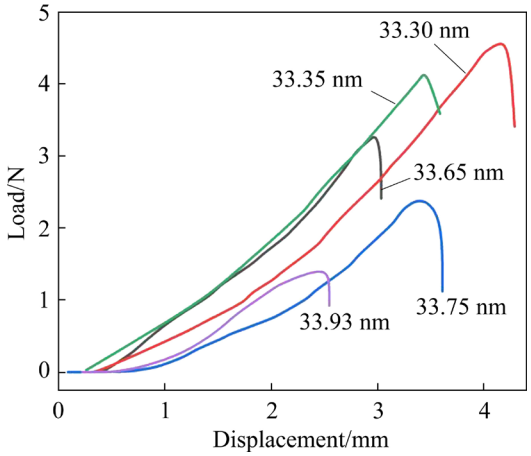

Fig. 9 Load-displacement curves of Cu foil

3.6 Surface roughness of Cu foils

A scanning electron microscope was used to examine the surface morphology of Cu foils. Figure 10 shows the surface roughness test results of Cu foils prepared using various Cr nucleated layers near the base surface, while Fig. 11 shows the surface profile of Cu foils prepared using various Cr nucleated layers near the base surface. Furthermore, we identified an intriguing phenomenon using SEM analysis: as the density of Cr nuclei increases, the surface roughness of Cu foils near the substrate can be reduced to a certain extent. The roughness of Cu foils near the substrate with Cr nucleus density of 2.61×10^9, 4.47×10^9, 5.00×10^9, 9.98×10^9, and 15.7×10^9 cm^{-2} density was found to be R_a=0.50 μm, R_a=0.42 μm, R_a=0.33 μm, R_a=0.29 μm, and R_a=0.21 μm, respectively. The surface roughness of copper foil containing 15.7×109 cm^{-2} Cr nuclei is 138% lower than that of copper foil containing 2.61×109 cm^{-2} Cr nuclei.

Cu foils with minimal surface roughness are required to reduce transmission signal loss [26−28]. In this study, increasing Cr nucleus density reduces the surface roughness of Cu foils near the substrate

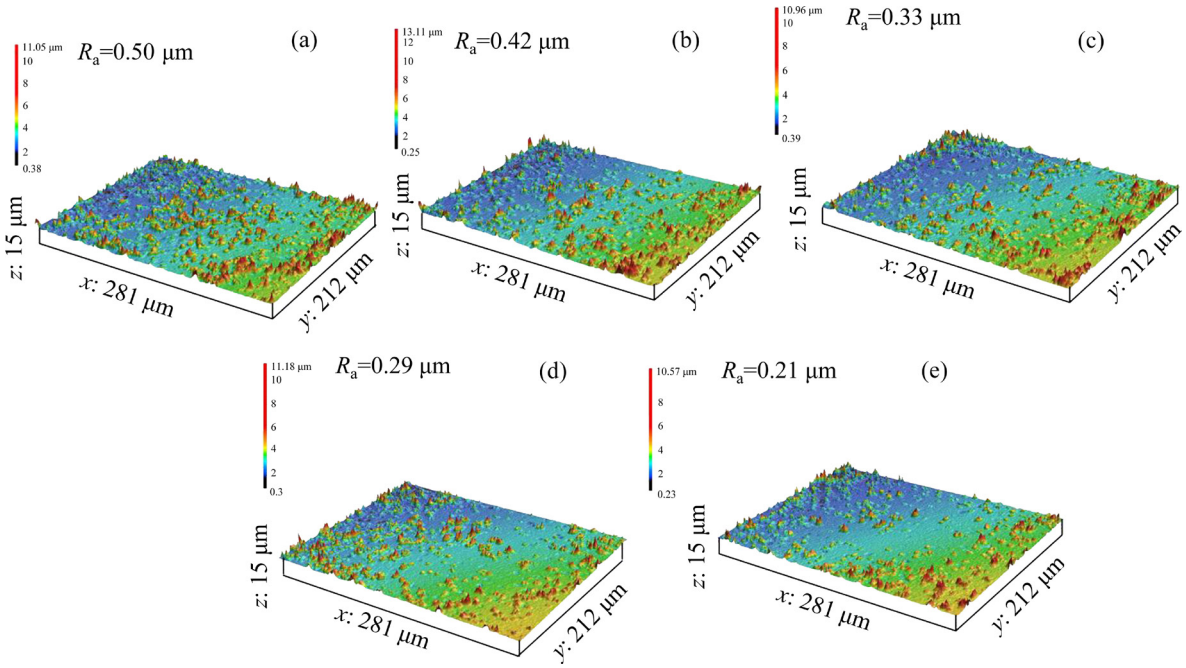

Fig. 10 Surface roughness of Cu substrate surfaces with Cr nucleus density of 2.61×10^9 cm^{-2} (a), 4.47×10^9 cm^{-2} (b), 5.00×10^9 cm^{-2} (c), 9.98×10^9 cm^{-2} (d), and 15.7×10^9 cm^{-2} (e)

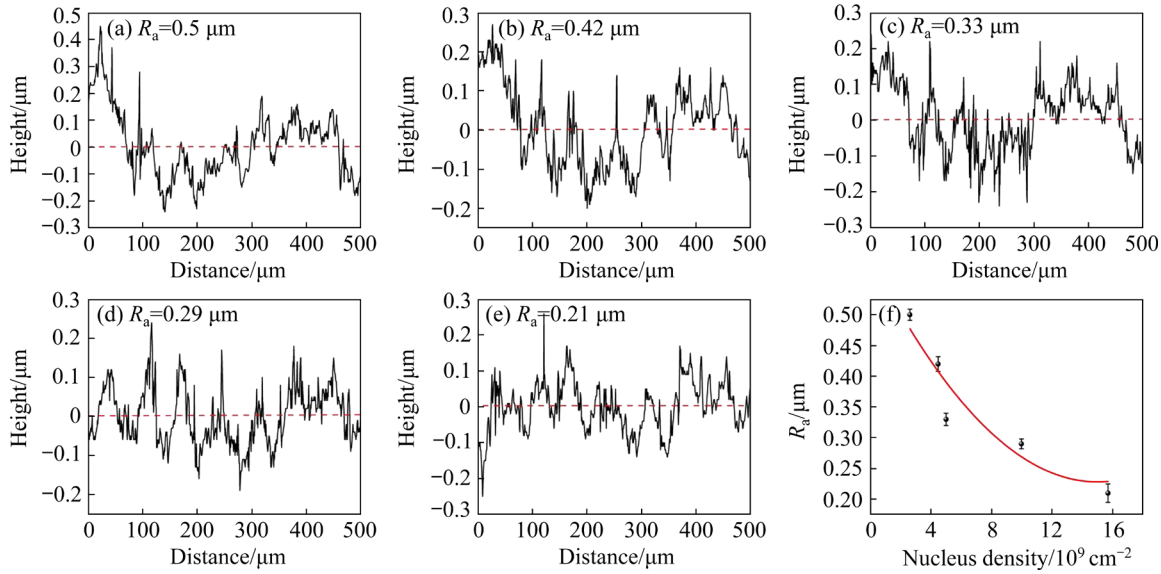

Fig. 11 Surface profiles of Cu foils near substrate with different Cr nucleus densities: (a−e) Surface profiles of Cu substrate surfaces with Cr nucleus density of 2.61×10^9 cm^{-2}, 4.47×10^9 cm^{-2}, 5.00×10^9 cm^{-2}, 9.98×10^9 cm^{-2}, and 15.7×10^9 cm^{-2}, respectively; (f) Variation trend of surface roughness with Cr nucleus density

to a certain extent. According to preliminary analysis, the reason is that the peeling performance of Cu foils is improved due to the increased density of Cr nuclei.

Furthermore, the surface roughness near the base of deposited copper foil is directly affected by the roughness of the base surface. Therefore, smoother Cu foils will be obtained by reducing the substrate surface roughness. It is an effective method for determining suitable Cr discrete nucleus density to achieve the ideal resistivity and roughness of Cu foils.

4 Discussion

4.1 Surface modification of Cu substrate by Cr nuclei

Figures 12(b−f) show the O 1s fitting spectra

of Cu substrate and its surfaces with Cr nucleus density of 2.61×10^9, 4.47×10^9, 5.00×10^9, 9.98×10^9, and 15.7×10^9 cm^{-2}, respectively. The peak-fitted O 1s signal of untreated Cu substrate has two components assigned to the C═O (532.0 eV) and C—O (533.3 eV) oxygen functionalities, as shown in Fig. 12(a). Combined with Figs. 12(b−f), it was found that as the thickness of Cr nucleus density

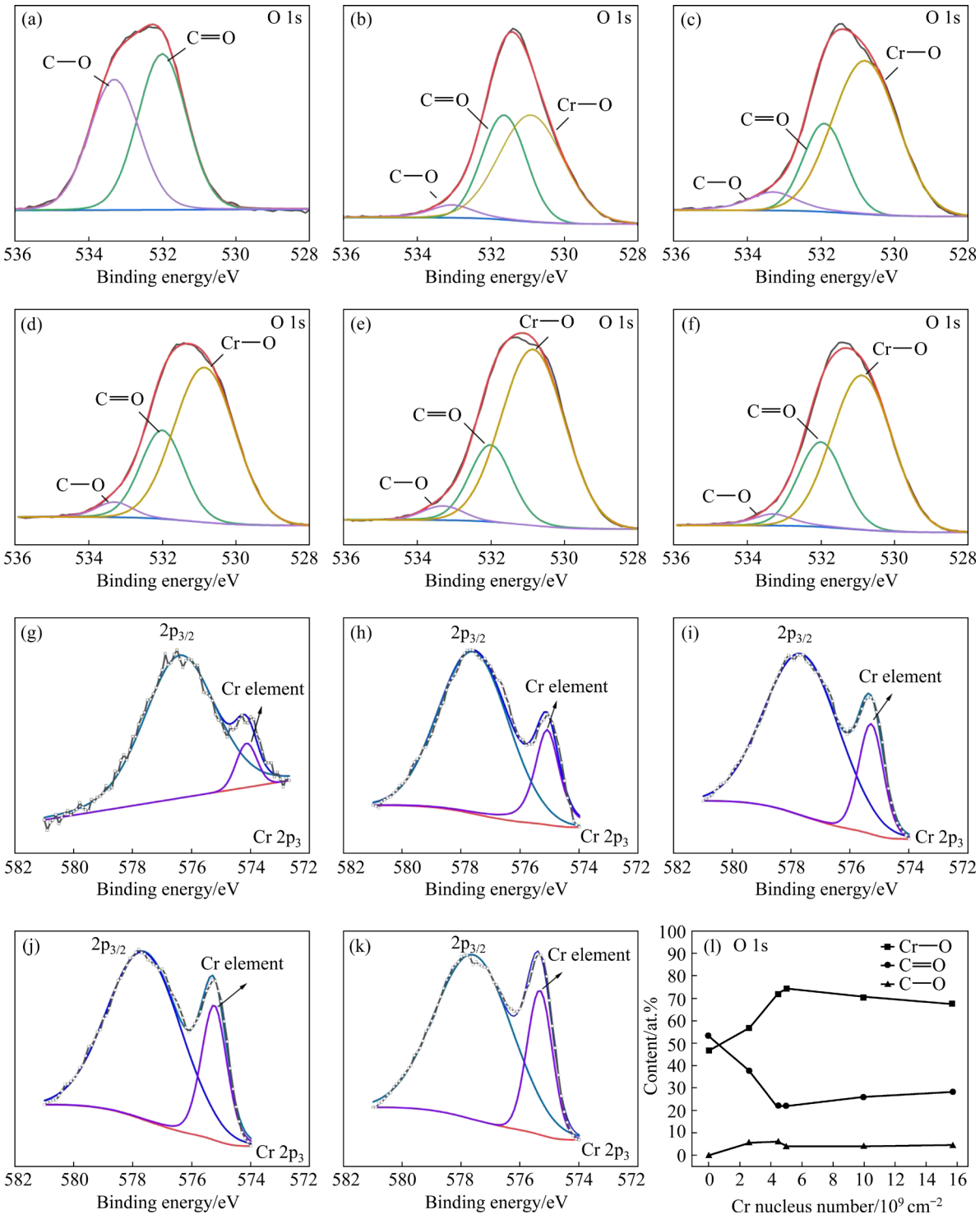

Fig. 12 O 1s spectra and peak fitting: (a) Cu substrate; (b) Cu substrate with Cr nucleus density of 2.61×10^9 cm^{-2}; (c) Cu substrate with Cr nucleus density of 4.47×10^9 cm^{-2}; (d) Cu substrate with Cr nucleus density of 5.00×10^9 cm^{-2}; (e) Cu substrate with Cr nucleus density of 9.98×10^9 cm^{-2}; (f) Cu substrate with Cr nucleus density of 15.7×10^9 cm^{-2}. (g−k) Cr $2p_3$ peak fitting of Cu substrate surfaces with Cr nucleus density of 2.61×10^9, 4.47×10^9, 5.00×10^9, 9.98×10^9, and 15.7×10^9 cm^{-2}, respectively; (l) Content of functional groups from O 1s spectrum (fitted as C—O, C═O, and Cr—O)

increases, the content of the C—O bond and C═O bond decreases, which is consistent with the signal detected by the C 1s spectrum, while the content of Cr—O (530.9 eV) bond increases. The presence of the corresponding Cr—O bond can be explained by the presence of Cr oxides, namely C_2O_3 [29,30]. C_2O_3 can reduce the surface energy of the substrate as well as the binding force between the substrate and the sedimentary layer, which is why the Cr discrete crystal core is conducive to copper foil stripping [14].

Cr_2O_3 has a good passivation effect on a Cu substrate, which is widely used to prevent metal corrosion. This is why potassium dichromate is still utilized despite its toxicity. We use hypotoxic chromium trivalent reduction of Cr nuclei. The Cr_2O_3 passivation layer can effectively reduce the binding force between the base and Cu foils, allowing for smooth stripping of Cu foils.

4.2 Effect of Cr nucleus density on stripping performance of Cu foils

The stress difference (internal stress) on both sides of ultra-thin copper foil directly affects its stripping performance. This difference is not only caused by electrodeposition but also by the influence of Cr discrete nuclei, which predominantly affects the stress of copper foil near the base side. Figure 2 shows the morphology of copper foil stripped with Cr nuclei deposited at different densities. It has been observed that as the density of Cr nuclei grows, so does the degree of crimping of Cu foil, which is reflected in the ease of stripping, indicating that the internal stress of Cu foil increases as the density of Cr nuclei increases. The average grain size of Cu foils can be estimated from the inner and outer grain sizes of copper foil by the XRD test.

The influence of Cr nucleus density on the internal stress of Cu foils can be analyzed using parameters like grain size and crystal plane spacing of Cu foils [31−34]. According to the Hoffman's internal stress expression [35−37]:

$$\sigma = \frac{E}{1-v} \cdot \frac{\Delta}{d} \tag{6}$$

where σ is the tensile stress of Cu foils; E is the elastic modulus of the coating (copper's elastic modulus is 119 GPa); v is Poisson's ratio (0.326 for Cu material); d is the grain size; Δ is the crystal plane spacing.

For the crystal plane (111), the stress is

$$\sigma = \frac{\sqrt{3}}{3} \cdot \frac{E}{1-v} \cdot \frac{a}{d} \tag{7}$$

For the crystal plane (200), the stress is

$$\sigma = \frac{\sqrt{2}}{8} \cdot \frac{E}{1-v} \cdot \frac{a}{d} \tag{8}$$

where a is the lattice constant.

The grain size of Cu foil is smaller near the substrate side than that on the far substrate side, indicating tensile stress, whereas the far base side indicates compressive stress. The change in stress with Cr discrete nucleus density is shown in Figs. 13(a) and (b), while Fig. 13(a) represents the stress of Cu foil far from base side, and Fig. 13(b)

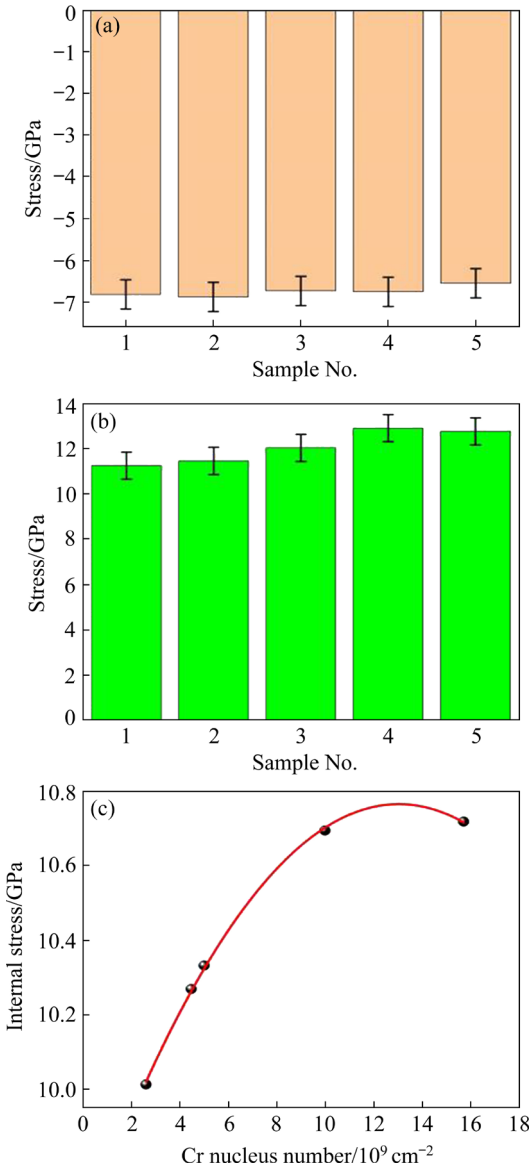

Fig. 13 Relation between grain size and stress of Cu foils: (a) Stress of Cu foil far from base side; (b) Stress of Cu foil near base side; (c) Variation trend of internal stress with Cr nucleus density

represents the stress of Cu foil near base side. The internal stress of Cu foil is the outward tensile stress. The variation trend of internal stress with Cr nucleus density is shown in Fig. 13(c). Figure 13(c) shows that as the density of Cr nucleus density increases, the internal stress of Cu foils increases.

Cr nuclei make the grain size of the Cu foil smaller and more uniform. This increases the tensile stress of the Cu foil during the stripping process, effectively improving the stripping performance of copper foil, which is consistent with the conclusion of Ref. (8).

TEM images of the Cu foil are shown in Fig. 14. Figures 14(a) and (b) show the bright-field TEM images of the Cu foil (Sample 1). Figures 14(c, d) show the bright-field TEM images of the Cu foil (Sample 5). TEM analysis shows that the grain sizes of Sample 1 and Sample 5 were 30.56 and 28.44 nm, respectively. Figure 14(b) shows high-resolution TEM (HRTEM) image of Sample 1, where the crystal lattice spacing of 0.207 nm corresponds to the (111) plane of Cu. Sample 5 (Fig. 14(d)) appears to have nanotwins. The nanotwins are caused by the bending deformation of the Cu foil. The nanotwins increase the strength of the Cu foil, which is consistent with tensile test results [8].

4.3 Effect of Cr nucleus density on electric conductivity of Cu foils

High resistance raises the temperature of electronic components [38]. It is critical to employ low resistivity Cu foils in lithium batteries and printed circuit boards. The resistivities of Cu foils prepared by Cr nuclei in the range of (4.91−5.20)×10^{-7} Ω·m. Three experiments were carried out to compare the conductivity of Cu foils prepared by Cr coating and potassium dichromate coating. Figure 15 shows the apparent morphology of substrates with electrodeposited Cr coating, Cr discrete nuclei, and potassium dichromate coating (Sample 1 is the substrate deposited with 0.67 μm Cr coating, Sample 2 is the substrate deposited with Cr discrete nuclei, and Sample 3 is the substrate coated with potassium dichromate coating). Compared to Cu foils coated with Cr or potassium

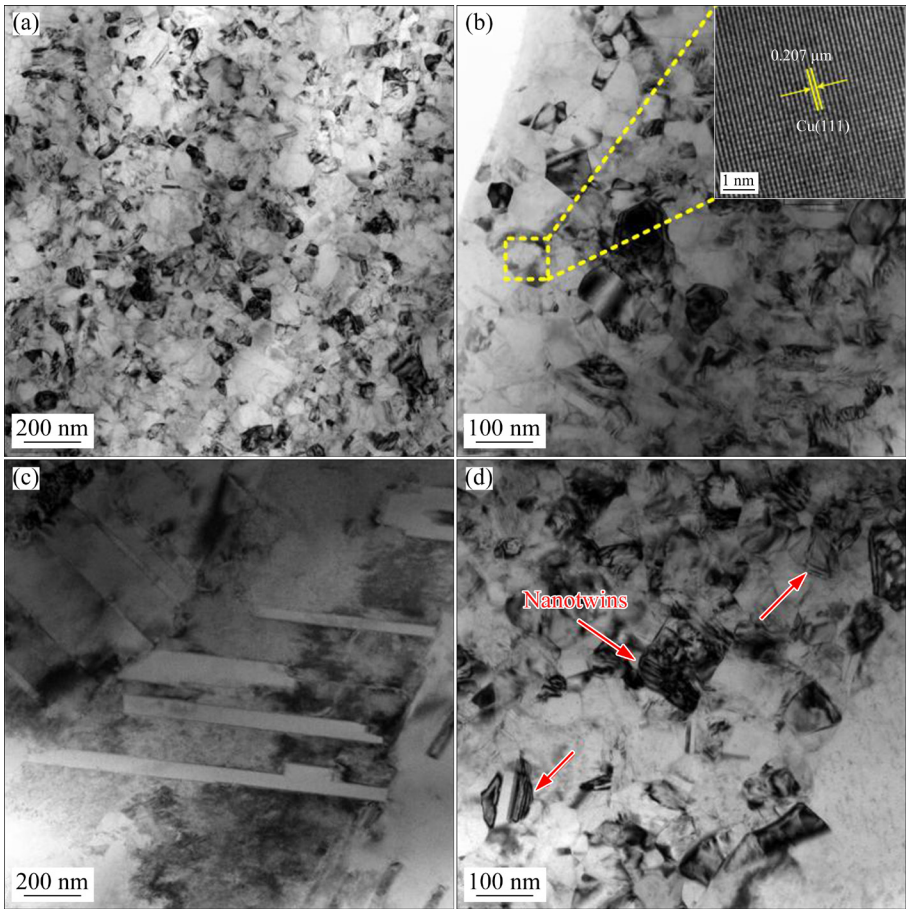

Fig. 14 Microstructure of Cu foil: (a) Bright-field TEM image of Cu foil (Sample 1); (b) HRTEM image of Cu foil (Sample 1); (c) Bright-field TEM image of Cu foil (Sample 5); (d) HRTEM image of Cu foil (Sample 5)

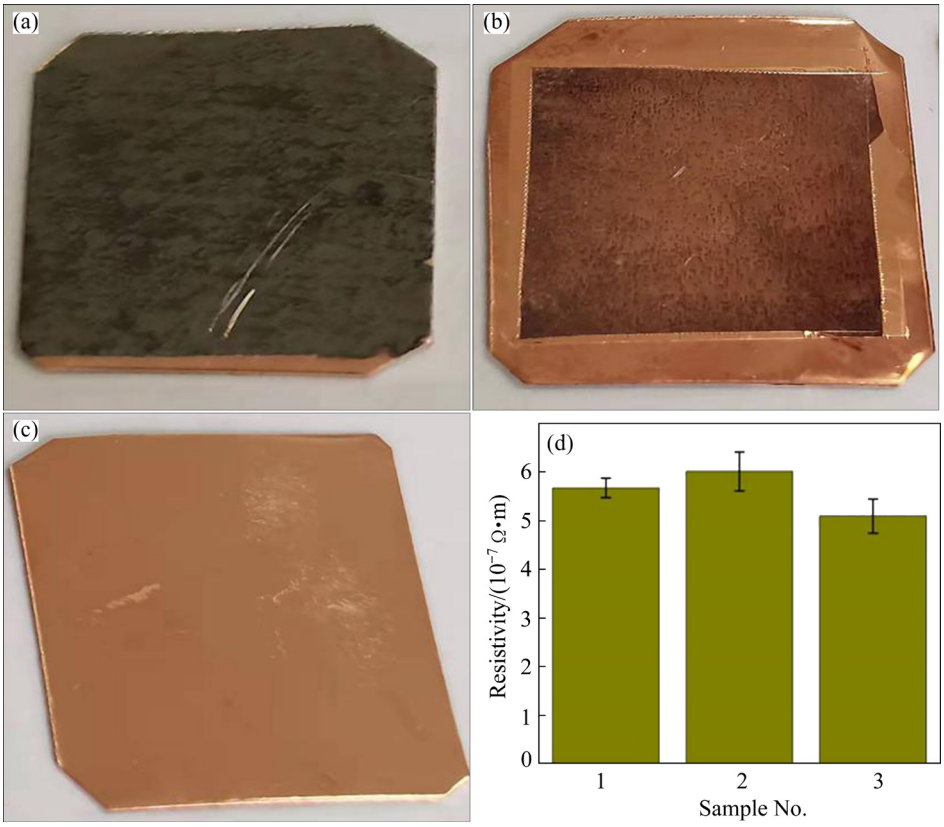

Fig. 15 Substrate morphology and resistivity of Cr coating layer, Cr nuclei, and potassium dichromate coating layer: (a) Substrate deposited with 0.67 μm Cr coating; (b) Substrate deposited with Cr discrete nucleus of 15.7×10^9 cm^{-2}; (c) Substrate coated with potassium dichromate coating; (d) Resistivity test results of Samples 1−3

dichromate, the Cu foils assisted by Cr discrete nuclei have lower average resistivity. The resistivity test results are shown in Fig. 15(d). According to recent literature, increasing the residual tensile stress of the film causes more severe grain deformation, an increase in grain boundary distortion, a more significant scattering of electrons induced by the grain boundary, and an increase in film resistivity [39,40]. As the density of Cr discrete nuclei increases, the residual tensile stress of Cu foil increases, which is the reason why Cr nuclei improve the resistivity of Cu foil.

5 Conclusions

(1) Cu foil with a thickness of 1.34 μm was prepared by reducing chromium trivalent to discrete Cr nano-nuclei on a Cu substrate. In addition to stripping ultra-thin Cu foil, the resistivity of Cu foil also reduced. Compared with Cr coating or potassium dichromate coating as the stripping layer, the Cu foil produced by uniformly distributed discrete Cr nano-nuclei has higher purity and better electrical conductivity. Discrete nuclei technology is a revolutionary approach for stripping ultra-thin Cu foil.

(2) The density of distinct Cr nano-nuclei influences the stripping effect of Cu foil. The degree of outward crimping of Cu foil increases as the density of discrete Cr nano-nuclei increases, and the greater the internal stress, the better the stripping effect of Cu foil. The roughness of the Cu foil near the base side decreases as the density of the Cr nuclei increases. When the density of discrete Cr nano-nuclei is 15.7×10^9 cm^{-2}, the corresponding roughness is 0.21 μm, which is the minimum. The density of the Cr discrete nuclei can be further tuned. Various Cu foil features can be regulated by altering the electrodeposition parameters, considering Cu foil's resistivity, roughness, and peel performance.

(3) Electrode position produces discrete nuclei that are suitable for conductive substrate materials. Conductive layers must be prepared by non-electrochemical methods such as physical deposition for non-conductive substrate materials.

Acknowledgments

The authors are grateful for the financial support from the National Natural Science Foundation of China (No. 52175407).

References

[1] YUE Y, LIANG H. Lithium-ion batteries: 3D current collectors for lithium-ion batteries: A topical review [J]. Small Methods, 2018, 2(8): 1800056.

[2] CHU H C, TUAN H Y. High-performance lithium-ion batteries with 1.5 μm thin copper nanowire foil as a current collector [J]. Journal of Power Sources, 2017, 346: 40−48.

[3] YEN C H, DOW W P. The influence of surface morphology of copper foils on the efficiency of lithium ion batteries [C]//ECS Meeting Abstracts. Maryland, USA: Electrochemical Society, 2017: 406.

[4] CHEN J Q, WANG X G, GAO H T, YAN S, CHEN S D, LIU X H, HU X L. Rolled electrodeposited copper foil with modified surface morphology as anode current collector for high performance lithium-ion batteries [J]. Surface and Coatings Technology, 2021, 410: 126881.

[5] MA X T, LIU Z T, CHEN H L. Facile and scalable electrodeposition of copper current collectors for high-performance Li-metal batteries [J]. Nano Energy, 2019, 59: 500−507.

[6] SONG G S, WANG Q, SUN L, LI S S, SUN Y F, FU Q, PAN C X. One-step synthesis of sandwich-type Cu/graphene/Cu ultrathin foil with enhanced property via electrochemical route [J]. Materials & Design, 2020, 191: 108629.

[7] YEN M H, LIU J H, SONG J M, LIN S C. Electrochemical corrosion properties of commercial ultra-thin copper foils [J]. Journal of Electronic Materials, 2017, 46(8): 5150−5157.

[8] WEI C L, YE N , HONG L K, YAO J H, XIA W Y, MAO J, WANG Y J, ZHAO Y C, TANG J C. Scalable preparation of ultrathin graphene-reinforced copper composite foils with high mechanical properties and excellent heat dissipation [J]. ACS Applied Materials & Interfaces, 2021, 13(18): 21714−21723.

[9] LEE B K, CHA K J, KWON T H. Fabrication of polymer micro/nano-hybrid lens array by microstructured anodic aluminum oxide (AAO) mold [J]. Microelectronic engineering, 2009, 86(4/5/6): 857−860.

[10] SHARMA S K. Green corrosion chemistry and engineering: Opportunities and challenges [M]. New Jersey: Wiley, 2012: 11−13.

[11] TAN Y H, WANG Y, ZHANG M, GAO J X, XU Q, TANG Y Z, YANG S P. Electrodeposited Zn−Ni−P−La alloys coating for electrolytic copper foil [J]. Chinese Journal of Applied Chemistry, 2015, 32(4): 458. (in Chinese)

[12] YANG G, LI Y, PI J, ZHU Q Q, CAI J W, HUANG Z J. Control of the adhesion strength between nickel replica and copper mold by electrochemical nucleation of lead [J]. Journal of Applied Electrochemistry, 2019, 49(10): 1003−1011.

[13] LI Y, YANG G, DENG D R, ZHANG Y Z. Effect of chromium coating thickness on surface adhesion of polyethylene terephthalate optical film [J]. Surfaces and Interfaces, 2021, 26: 101429.

[14] YANG G, CHEN J, LI B, WANG Q F, ZHANG Y Z, PI J. Impact of Cr nanocrystalline discrete crystal nuclei on demolding strength and surface roughness of precision electroforming Ni layer on Cu substrate [J]. Journal of Applied Electrochemistry, Journal of Applied Electrochemistry, 2022, 52(7): 1091−1100.

[15] MAJD M T, SHAHRABI T, RAMEZANZADEH B. The role of neodymium based thin film on the epoxy/steel interfacial adhesion and corrosion protection promotion [J]. Applied Surface Science, 2019, 464: 516−533.

[16] TODESCHINI M, BASTOS DA SILVA FANTA A, JENSEN F, WAGNER J B, HAN A D. Influence of Ti and Cr adhesion layers on ultrathin Au films [J]. ACS Applied Materials & Interfaces, 2017, 9(42): 37374−37385.

[17] WU W P, HUANG J Q, NÄTHER J, OMAR N A B, KÖSTER F LAMPKE T, LIU Y X, PAN H J, ZHANG Y. Texture orientation, morphology and performance of nanocrystalline nickel coatings electrodeposited from a Watts-type bath: Effects of H_3BO_3 concentration and plating time [J]. Surface and Coatings Technology, 2021, 424: 127648.

[18] SARAC U, BAYKUL M C. Morphological and microstructural properties of two-phase Ni−Cu films electrodeposited at different electrolyte temperatures [J]. Journal of Alloys and Compounds, 2013, 552: 195−201.

[19] HACIISMAILOGLU M, ALPER M. Effect of electrolyte pH and Cu concentration on microstructure of electrodeposited Ni−Cu alloy films [J]. Surface and Coatings Technology, 2011, 206(6): 1430−1438.

[20] NASIRPOURI F, SANAEIAN M R, SAMARDAK A S, SUKOVATITSINA E V, OGNEV A V, CHEBOTKEVICH L A, HOSSEINI M G, ABDOLMALEKI M. An investigation on the effect of surface morphology and crystalline texture on corrosion behavior, structural and magnetic properties of electrodeposited nanocrystalline nickel films [J]. Applied Surface Science, 2014, 292: 795−805.

[21] SAJJADNEJAD M, OMIDVAR H, JAVANBAKHT M, MOZAFARI A. Textural and structural evolution of pulse electrodeposited Ni/diamond nanocomposite coatings [J]. Journal of Alloys and Compounds, 2017, 704(15): 809−817.

[22] XUE Z M, LEI W N, WANG Y Q, QIAN H F, LI Q L Effect of pulse duty cycle on mechanical properties and microstructure of nickel-graphene composite coating produced by pulse electrodeposition under supercritical carbon dioxide [J]. Surface and Coatings Technology, 2017, 325: 417−428.

[23] HALL E O. The deformation and ageing of mild steel: III discussion of results [J]. Proceedings of the Physical Society. Section B, 1951, 64(9): 747−753.

[24] PETCH N J. The cleavage strength of polycrystals [J]. Journal of the Iron and Steel Institute, 1953, 174: 25−28.

[25] HE W L, MENG B, SONG B Y, WAN M. Grain size effect on cyclic deformation behavior and springback prediction of Ni-based superalloy foil [J]. Transactions of Nonferrous Metals Society of China, 2022, 32(4): 1188−1204.

[26] LU L L, GE J, YANG J N, CHEN S M, YAO H B, ZHOU F, YU S H. Free-standing copper nanowire network current

collector for improving lithium anode performance [J]. Nano Letters, 2016, 16(7): 4431−4437.
[27] PARK H, UM J H, CHOI H, YOON W S, SUNG Y E., CHOE H. Hierarchical micro-lamella-structured 3D porous copper current collector coated with tin for advanced lithium-ion batteries [J]. Applied Surface Science, 2017, 399: 132−138.
[28] BASU N, DUTTA A, SINGH R, BAYAZEED M, PARMAR A S, SOM T, LAHIRI J. Substrate roughness and crystal orientation-controlled growth of ultra-thin BN films deposited on Cu foils [J]. Applied Physics A, 2022, 128(5): 1−10.
[29] ARDELEAN H, PETIT S, LAURENS P, MARCUS P, AREFI-KHONSARI F. Effects of different laser and plasma treatments on the interface and adherence between evaporated aluminium and polyethylene terephthalate films: X-ray photoemission, and adhesion studies [J]. Applied Surface Science, 2005, 243(1/2/3/4): 304−318.
[30] UNGER W E S, LIPPITZ A, GROSS T, FRIEDRICH J F, WÖLL C, NICK L. The use of octadecyltrichlorosilane self-assembled layers as a model for the assessment of plasma treatment and metallization effects on polyolefins [J]. Langmuir, 1999, 15(4): 1161−1166.
[31] BOIJOUX R, PARRY G, FAOU J Y, COUPEAU C. How soft substrates affect the buckling delamination of thin films through crack front sink-in [J]. Applied Physics Letters, 2017, 110(14): 141602.
[32] FAOU J Y, GRACHEV S, BARTHEL E, PARRY G. From telephone cords to branched buckles: A phase diagram [J]. Acta Materialia, 2017, 125: 524−531.
[33] BOIJOUX R, PARRY G, COUPEAU C. Buckle depression as a signature of Young's modulus mismatch between a film and its substrate [J]. Thin Solid Films, 2018, 645: 379−382.
[34] ŽÁK S, LASSNIG A, CORDILL M J, PIPPAN R. Finite element-based analysis of buckling-induced plastic deformation [J]. Journal of the Mechanics and Physics of Solids, 2021, 157: 104631.
[35] FINEGAN J D, HOFFMAN R W. Stress anisotropy in evaporated iron films [J]. Journal of Applied Physics, 1959, 30(4): 597−598.
[36] HOFFMAN R W. Stresses in thin films: The relevance of grain boundaries and impurities [J]. Thin Solid Films, 1976, 34(2): 185−190.
[37] ABADIAS G, CHASON E, KECKES J, SEBASTIANI M, THOMPSON G B, BARTHEL E, DOLL G L, MURRAY C E, STOESSEL C H, MARTINU L. Stress in thin films and coatings: Current status, challenges, and prospects [J]. Journal of Vacuum Science & Technology A: Vacuum, Surfaces, and Films, 2018, 36(2): 020801.
[38] MEHTA R, CHUGH S, CHEN Z H. Enhanced electrical and thermal conduction in graphene-encapsulated copper nanowires [J]. Nano Letters, 2015, 15(3): 2024−2030.
[39] TSENG W T, WANG Y L, NIU J. Microstructure-related resistivity change after chemical−mechanical polish of Al and W thin films [J]. Thin Solid Films, 2000, 370: 96−100.
[40] TANG W, XU K W, WANG P, LI X. Residual stress and crystal orientation in magnetron sputtering Au films [J]. Materials Letters, 2003, 57: 3101−3106.

离散铬纳米核对超薄铜箔剥离性能和电阻率的影响

杨 光[1]，惠 越[1]，陈 菊[1]，李 波[1]，陈建华[2]，刘 铠[2]，梁桂德[2]，邓丁榕[1]

1. 集美大学 海洋设备与机械工程学院，厦门 361021；
2. 福建夜光达科技有限公司，晋江 362241

摘 要：提出一种利用电化学沉积法制备 Cr 纳米离散晶核实现超薄铜箔剥离的策略。结果表明，该方法可以制备厚度约为 1.34 μm 的铜箔。Cr 纳米离散晶核密度直接影响铜箔的剥脱性能、表面粗糙度和电阻率。当 Cr 纳米离散晶核密度为 15.7×10^9 cm^{-2} 时，铜箔的剥离性能最好，电阻率为 4.95×10^{-7} Ω·m，比常规厚度为 0.67 μm Cr 涂层的电阻率低 9.2%，比重铬酸钾涂层的电阻率低 15.8%，抗拉强度超过 248.80 MPa。

关键词：电沉积；铜箔；离散纳米核；剥离；电阻率

(Edited by Xiang-qun LI)